Conductance of metallic nanoribbons with defects*

Deng Shi-Xian(邓诗贤) and Liang Shi-Dong(梁世东)†

State Key Laboratory of Optoelectronic Material and Technology and Guangdong Province Key Laboratory of Display Material and Technology, School of Physics and Engineering, Sun Yat-Sen University, Guangzhou 510275, *China*

(Received 3 October 2011; revised manuscript received 17 November 2011)

The conductances of two typical metallic graphene nanoribbons with one and two defects are studied using the tight binding model with the surface Green's function method. The weak scattering impurities, $U \sim 1$ eV, induce a dip in the conductance near the Fermi energy for the narrow zigzag graphene nanoribbons. As the impurity scattering strength increases, the conductance behavior at the Fermi energy becomes more complicated and depends on the impurity location, the AA and AB sites. The impurity effect then becomes weak and vanishes with the increase in the width of the zigzag graphene nanoribbons (150 nm). For the narrow armchair graphene nanoribbons, the conductance at the Fermi energy is suppressed by the impurities and becomes zero with the increase in impurity scattering strength, $U > 100$ eV, for two impurities at the AA sites, but becomes constant for the two impurities at the AB sites. As the width of the graphene nanoribbons increases, the impurity effect on the conductance at the Fermi energy depends sensitively on the vacancy location at the AA or AB sites.

Keywords: conductance, graphene nanoribbon, defects

PACS: 73.63.–b, 72.80.Vp, 72.10.Fk **DOI:** 10.1088/1674-1056/21/4/047306

1. Introduction

Graphene, as a new kind of low-dimensional material, has attracted much attention, not only for potential applications in new kinds of devices, but also for understanding some of the fundamental physics in nanoscale materials.[1] The mobile electrons in graphene behave as massless Dirac fermions due to their unique honeycomb structures, and the geometry of sp^2 carbon networks has strongly influenced its electronic band structure with a linear dispersion relation near the Dirac point.[2−4] Due to the chiral nature of charge excitations, many unconventional quantum transport features are exhibited, such as anomalous quantum Hall effects.[5,6]

In particular, quasi-one-dimensional graphene nanoribbons (GNRs) with different edges can be obtained by cutting two-dimensional (2D) graphene sheets along different directions. There are two typical edge shapes in GNRs, called zigzag and armchair, respectively. The electronic properties of GNRs have triggered great enthusiasm for their study. GNRs can be either semiconducting or metallic, depending on their shape.[7] All zigzag GNRs are metallic, but armchair GNRs are metallic only when their width satisfies the condition $N = 3n - 1$, where n is an integer and N is the number of A(B)-site atoms in a unit cell, relating to the width of the GNRs (see Fig. 1).[7] In addition, edge states exist in zigzag GNRs, but not armchair GNRs.[8]

Physically, defects and impurities play an important role in such nanoscale materials. The conductance of GNRs with edge defects exhibits zero dips,[9,10] and the vacancies in GNRs lead to conductance suppression and resonance.[11−14] However, there are usually many defects or impurities in GNRs. In the present paper, we investigate the transport properties of metallic zigzag and armchair GNRs with two defects. The paper is organized as follows. Firstly, the model and the method are briefly introduced in Section 2. Then, we show our results and discussions in Section 3, and finally we give a conclusion in Section 4.

2. Model and method

The geometries of zigzag and armchair GNRs are shown in Fig. 1. There are two inequivalent sublattices, called A- and B-sublattices, respec-

*Project supported by the National Natural Science Foundation of China (Grants Nos. 10774194 and 51072236), the Elite Student Program from National Education Department, and the Fundamental Research Funds for the Central Universities.

†Corresponding author. E-mail: stslsd@mail.sysu.edu.cn

© 2012 Chinese Physical Society and IOP Publishing Ltd

tively. The graphene lattice constant is $a_0 = 2.49$ Å (1 Å=0.1 nm)[9,15] and the lengths of the zigzag and armchair GNRs are $L_{\rm zig} = Ma_0$ and $L_{\rm arm} = \sqrt{3}Ma_0$, respectively, where M is the number of unit cells in the ribbon. The width of zigzag GNRs can be written as $W_{\rm zig} = \sqrt{3}/2Na_0$, while the width of armchair GNRs are $W_{\rm arm} = Na_0/2$. The atoms in a unit cell are denoted by 1A, 1B,..., NA, NB as shown in Fig. 1.[9]

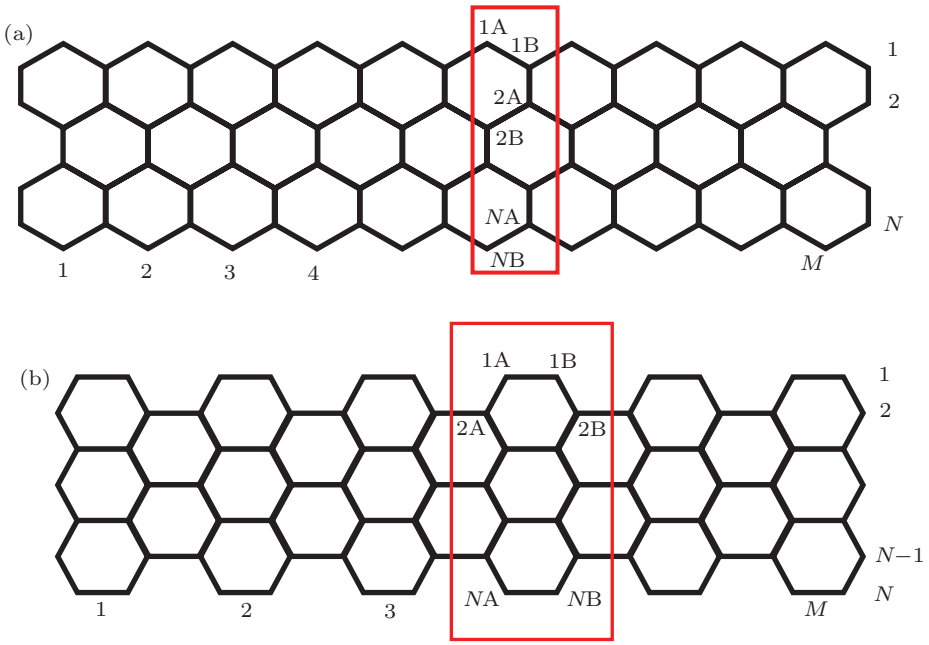


Fig. 1. (colour online) The geometry of GNRs: (a) a zigzag GNR ($N = 4$), and (b) an armchair GNR ($N = 7$). The honeycomb structure is composed of two sublattices, A and B. The red rectangle denotes a unit cell.

The basic transport properties of graphene are dominated by the π electrons in graphene. We can use the nearest-neighbor π tight-binding model to describe a GNR with defects. The Hamiltonian reads

$$H = -t\sum_{\langle i,j\rangle}\left(c_i^{\dagger}c_j + \text{h.c.}\right) + U\sum_{l} c_l^{\dagger}c_l, \qquad (1)$$

where t is the nearest-neighbor hopping parameter, $t \approx 2.66$ eV, and U represents the strength of defects, set to infinity for vacancies but a small value for weak scatters.[11−14] We assume all edge sites are terminated by hydrogen atoms.

The transport system we consider includes the left lead, conductor, and the right lead. The left- and right-leads are semi-infinite perfect GNRs with the same edge shape as the middle conductor. The transport conductance can be calculated based on the Landauer formula with the surface Green's function method. The transport conductance of the system can be written as[9,16,17]

$$G(E) = \frac{2e^2}{h}T(E) = \frac{2e^2}{h}\,\text{Tr}\left[\Gamma^{\rm L}G_r\Gamma^{\rm R}G_r^{+}\right], \qquad (2)$$

where $T(E)$ is the transmission coefficient, and $\Gamma^{\rm L(R)}$ describes the rate of electron escape from the left lead to the conductor and then to the right lead. They can be expressed as

$$\Gamma^{\rm L(R)} = \text{i}\left[\Sigma^{\rm L(R)} - \left(\Sigma^{\rm L(R)}\right)^{+}\right], \qquad (3)$$

where

$$\Sigma^{\rm L} = H_{0,1}^{+}g_{0,0}^{\rm L}H_{0,1}, \qquad (4)$$

$$\Sigma^{\rm R} = H_{1,2}g_{2,2}^{\rm R}H_{1,2}^{+} \qquad (5)$$

is the self-energy of the coupling between the leads and the conductor. The Green's function of the system G_r can be expressed in terms of[9,16−18]

$$G_r = [(E + \text{i}\eta)I - H_{1,1} - \Sigma^{\rm L} - \Sigma^{\rm R}]^{-1}. \qquad (6)$$

Using the recursive Green's function method with the iterative technique, we can calculate the surface Green's function and the transmission probability of the system.[9] The surface retarded Green's functions of the left lead are $g_{0,0}^{\rm L}$ and right lead $g_{M+1,M+1}^{\rm R}$, via an iterative procedure.[19]

$$g_{0,0}^{\rm L} = [(E + \text{i}\eta)I - H_{0,0} - H_{-1,0}^{+}\tilde{\Lambda}]^{-1}. \qquad (7)$$

$$g^{\rm R}_{M+1,M+1} = [(E+{\rm i}\eta)I - H_{0,0} - H^{+}_{-1,0}\Lambda]^{-1}, \quad (8)$$

where the Λ and $\tilde{\Lambda}$ are

$$\Lambda = p_0 + \tilde{p}_0 p_1 + \tilde{p}_0\tilde{p}_1 p_2 + \cdots + \tilde{p}_0\tilde{p}_1\tilde{p}_2\cdots p_n, \quad (9)$$

$$\tilde{\Lambda} = p_0 + p_0\tilde{p}_1 + p_0 p_1\tilde{p}_2 + \cdots + p_0 p_1 p_2\cdots\tilde{p}_n, \quad (10)$$

where p_i and $\tilde{p}_i$ are defined as follows:

$$p_i = \left(I - p_{i-1}\tilde{p}_{i-1} - \tilde{p}_{i-1}p_{i-1}\right)^{-1} p^2_{i-1}, \quad (11)$$

$$\tilde{p}_i = \left(I - p_{i-1}\tilde{p}_{i-1} - \tilde{p}_{i-1}p_{i-1}\right)^{-1} \tilde{p}^2_{i-1}. \quad (12)$$

The initialized values are calculated by

$$p_0 = \left[(E+{\rm i}\eta)\, I - H_{0,0}\right]^{-1} H^{+}_{-1,0}, \quad (13)$$

$$\tilde{p}_0 = \left[(E+{\rm i}\eta)\, I - H_{0,0}\right]^{-1} H_{-1,0}, \quad (14)$$

where $H_{j,j}$ is the Hamiltonian of the j-th cell and $H_{j,j+1}$ is the coupling matrix of the nearest neighbor j-th and $(j+1)$-th cells. η is infinitesimal $\eta \to 0^+$ and I is a unit matrix. The remaining Green's function $g^{\rm R}$ is calculated layer by layer, going down from $l = M$ to $l = 2$,[19]

$$g^{\rm R}_{l,l} = \left[(E+{\rm i}\eta) - H_{l,l} - H_{l,l+1}g^{\rm R}_{l+1,l+1}H^{+}_{l,l+1}\right]. \quad (15)$$

3. Results and discussion

As a typical GNR with two defects, we mainly focus on two kinds of defects, weak scattering impurities and vacancies. Suppose that two defects are located in the same unit cell of the GNR and their positions are within the half width for simplicity, we consider that the number of A (B)-site atoms in a unit cell is $N = 8$ and the number of unit cells is $M = 300$. We use iA (iB)-site to denote an impurity or defect located at the iA (iB)-site and the iAjA (iAjB), where $i \neq j$ denotes one defect located on the iA-site and the other at the jA (jB)-site, respectively.

3.1. A zigzag GNR

We first investigate the effect of the weak scattering impurity in the GNR. We compare the conductances of the pure zigzag GNR and one- or two-impurity GNRs, as shown in Fig. 2. The conductance of a pure zigzag GNR is flat at the Fermi energy, exhibiting metallic behavior. For an impurity at 1A, the conductance has a dip near the Fermi energy (see Fig. 1(a)), which agrees with Li's results.[9] For two impurities at 1AjA, where $j = 2 \sim 4$, the conductances have two dips near the Fermi energy (see Fig. 1(a)). However, as the location of the impurity is far away from the edge, the dip at the Fermi energy gradually disappears. Then the conductance of the 1AjA type behaves similarly to the case of the 1A type, exhibiting only one dip near the Fermi energy. In addition, for the 1AjB type, the conductance also has only one dip near Fermi energy, as shown in Fig. 2(b). For the two impurities located at the bulk sites, the 2AjA (2AjB) type, the conductances show only one dip, as depicted in Figs. 2(c) and (d), where $j = 1 \sim 4$. Due to the nonbonding nature of edge states in the zigzag GNR,[7] the electronic states of the edge sites are almost localized. For impurities at the same sublattice as the edge sites, especially near the corresponding edge, there exists scattering between impurities and electrons, which affects the conductance of the system. Therefore, the conductance of a zigzag GNR with two impurities depends on the location of the impurities, and the width of the GNR. The position of the conductance dip is similar to the case of a single impurity at the jA-site.

For the vacancy defects, the conductances of all cases (one or two vacancies) are symmetric to the Fermi energy, which is different from the cases of two impurities. The details of the conductance depends on the location of the vacancies. In Fig. 3(a), we plot the conductances in different energy channels near the Fermi energy for the one vacancy at 1A and the two vacancies at 1AjA, where $j = 2 \sim 4$. For one vacancy at the 1A site, the conductance has two dips at $\pm$1.3 eV. For the 1AjA type vacancies there are four zero-conductance dips and three local maximums at different energy channels. One of the local conductance maximums is located at the Fermi energy. For the 1AjB type vacancies (Fig. 3(b)), there are only three dips in the conductances. One is located at the Fermi energy, and the others are at two symmetric energy channels near $\pm$1.3 eV. The conductance dips become shallow as the position of the B-sublattice impurity j locates beyond the A-sublattice impurity. It can be seen from Figs. 3(a) and 3(b) that the influences of the two vacancies located at the 1AjA and 1AjB are quite different, especially near the Fermi energy. Interestingly, for the 2AjA vacancies shown in Fig. 3(c), the conductance behaviors in the different

energy channels are also quite different. Particularly, the conductances for the 2A and 2A3A vacancies have a maximum at the Fermi energy, while for the 2A4A vacancy, the conductance has a minimum at the Fermi energy. Moreover, for the 2AjB vacancies shown in Fig. 3(d), as the vacancy at the B-sublattice moves beyond the vacancy at the 2A site, the conductance shows a dip in the Fermi energy.

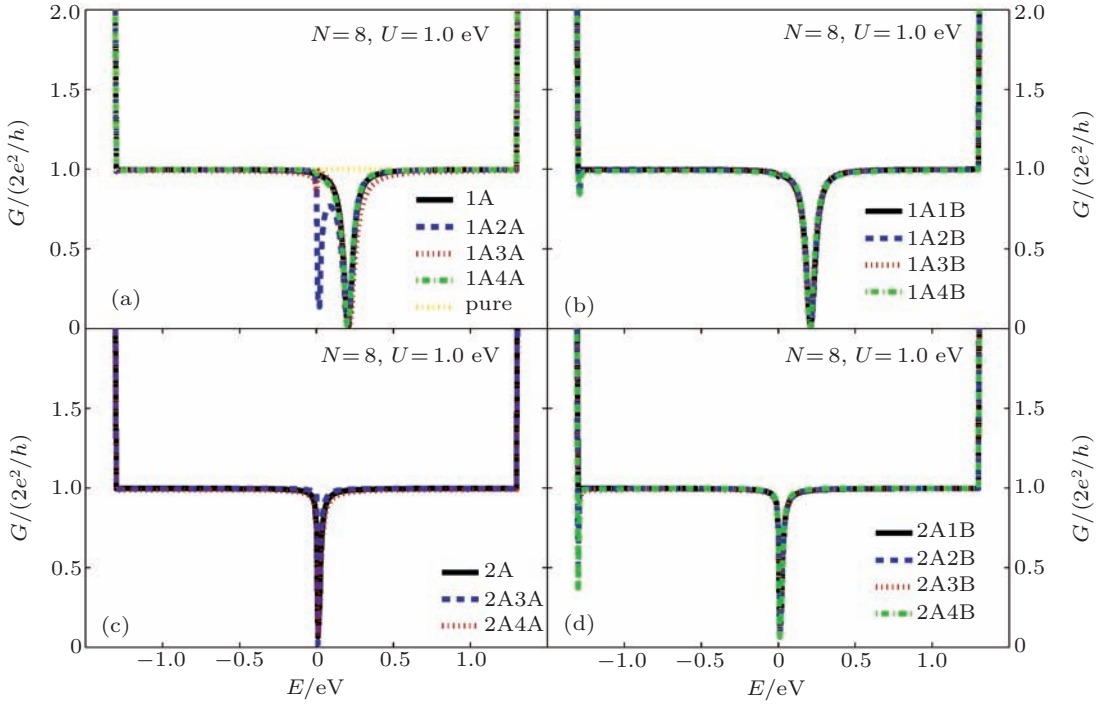


Fig. 2. (colour online) The conductance of the zigzag GNR (N = 8) near the Fermi energy. (a) One impurity is located at the 1A site and two impurities at the 1AjA sites (pure means without impurities for comparison); (b) two impurities located at the 1AjB sites; (c) one impurity located at the 2A, and two impurities at the 2AjA sites; and (d) two impurities located at the 2AjB sites.

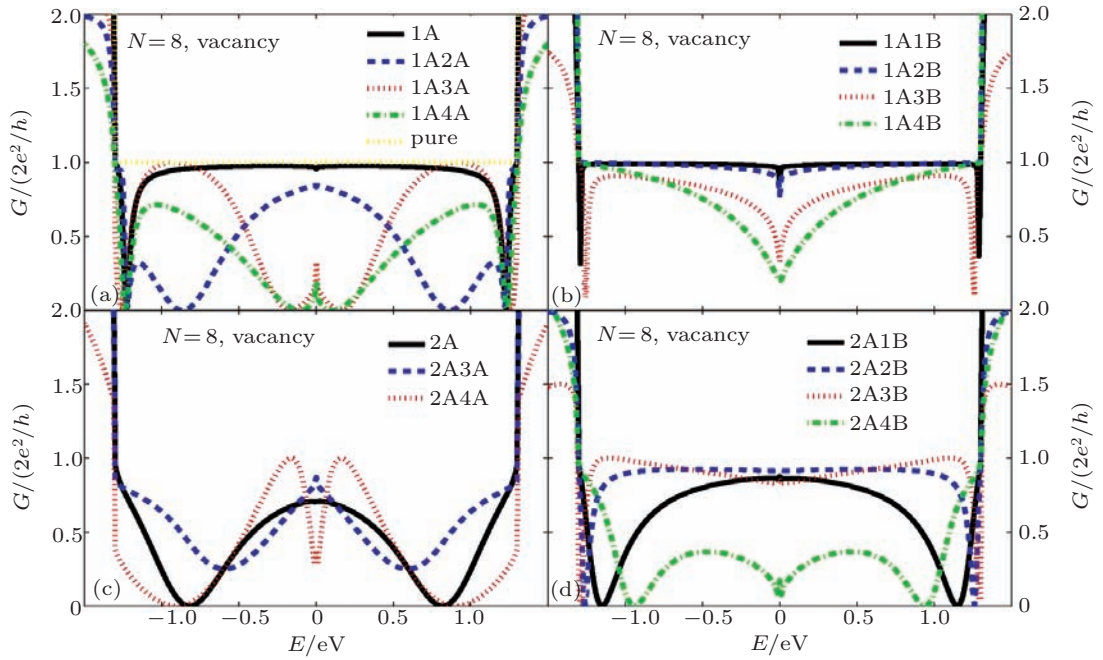


Fig. 3. (colour online) The conductance of the zigzag GNR (N = 8) near the Fermi energy. (a) One vacancy at the 1A site and two vacancies located at the 1AjA sites (pure for comparison); (b) two vacancies located at the 1AjB sites; (c) one vacancy located at the 2A site, and two vacancies at the 2AjA sites; and (d) two vacancies located at the 2AjB sites.

A single vacancy at the A(B)-site in the graphene sheet leads to the amplitude of wave function vanishing at the A(B)-sublattice and forms a zero-energy quasilocalized state around the vacancy, which belongs to the B(A) sublattice, i.e. nonbonding character.[10,20] Thus, when the single vacancy is near the corresponding edge at the same sublattice,[10] e.g. 1A-site vacancy, the coupling between vacancy states and edge states forms the bonding and antibonding configuration, resulting in two conductance dips. However, if the single vacancy is far away from the corresponding edge, e.g. 1B-site vacancy, the conductance has only one dip near the Fermi energy. For double vacancies, there are four conductance dips for the 1AjA type and three dips for the 1AjB type. This is because there is one vacancy located at the edge for both of the two types of vacancies, and the coupling between the vacancy state and the edge state is stronger than the coupling between the two vacancies. However, when the two vacancies are located in the bulk, the interplay between the two vacancies makes the resonance of the conductance more complicated, e.g. 2AjA type. In addition, it is easy to find that the conductance at the Fermi energy decreases with the increase in distance between the two vacancies.

In order to investigate the effect of the scattering strength of the defects, we plot the conductance at the Fermi energy versus the scattering strength of defects in Fig. 4. One impurity located at the 1A site and two AA-type defects located at 1AjA, where $j = 2 \sim 4$, are shown in Fig. 4(a). The conductances at the Fermi energy smoothly decrease for $U < 100$ eV and become stable for $U > 100$ eV with the increasing in the scattering strength. For AB-type defects located at 1AjB where $j = 1 \sim 4$ in Fig. 4(b), the conductances at the Fermi energy show one dip with the increasing in the scattering strength, and the minimums of the conductances depend on the location of the defect at the B-sublattice. For the 2A and 2AjA type impurities in Fig. 4(c) and the 2AjB impurities in Fig. 4(d), the behaviors of the conductances are similar to the cases in Figs. 4(a) and 4(b).

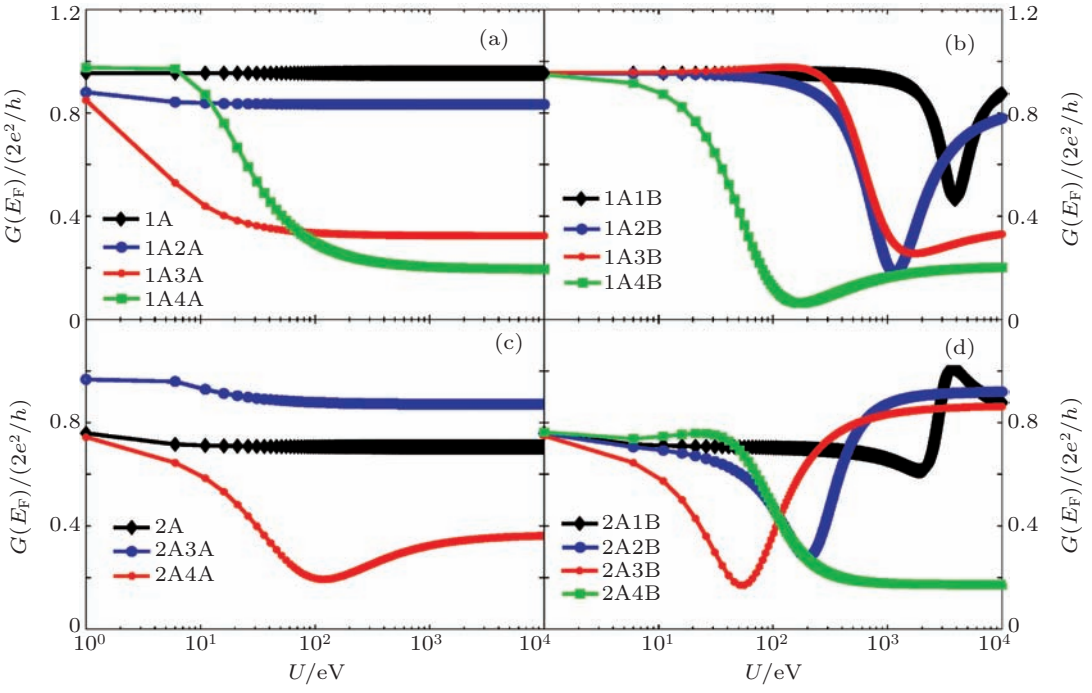


Fig. 4. (colour online) The conductance of the zigzag GNR ($N = 8$) at the Fermi energy versus the impurity scattering strength. (a) One impurity located at the 1A site and two at the 1AjA sites; (b) two impurities located at the 1AjB sites; (c) one impurity located at the 2A, and two impurities at the 2AjA sites; and (d) two impurities located at the 2AjB sites.

Another interesting question is how the behavior of the conductance relates to the width of the GNR. In Fig. 5, we investigate the conductances at the Fermi energy versus the number of A (B)-site atoms that are related to the width of the GNR. The conductances at the Fermi energy for all vacancy cases converge to near 1. This implies that the effect of the vacancy vanishes as the width of the GNR becomes large.

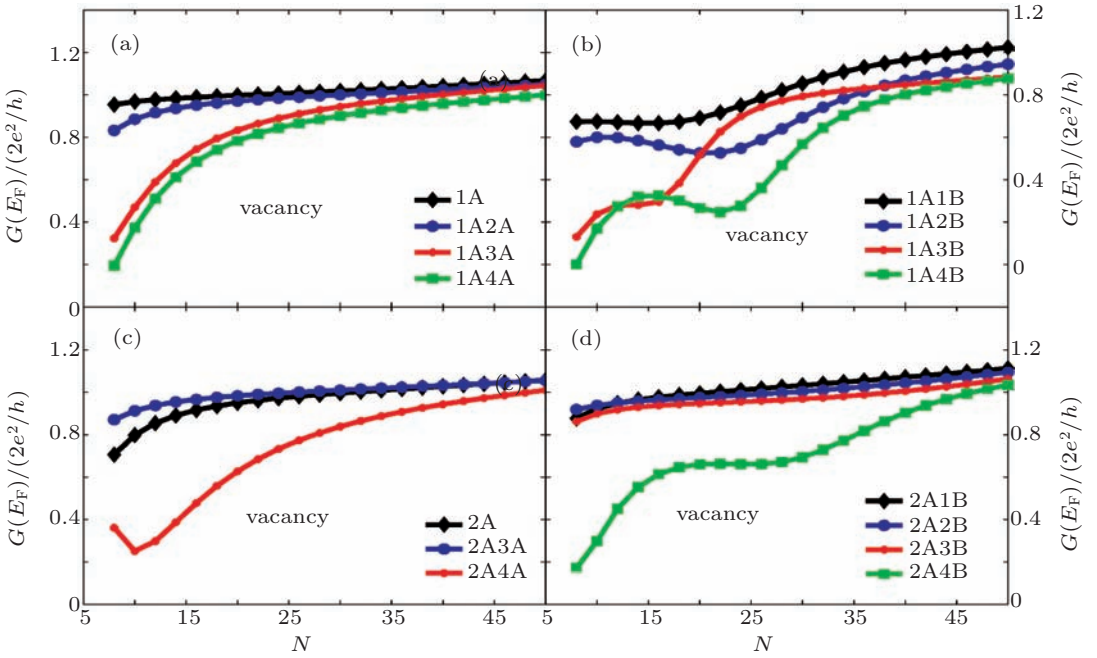


Fig. 5. (colour online) The conductance of the zigzag GNR at the Fermi energy versus the width of the GNR. (a) One vacancy at the 1A site and two vacancies located at the 1AjA sites; (b) two vacancies located at the 1AjB sites; (c) one vacancy located at the 2A site, and two vacancies at the 2AjA sites; and (d) two vacancies located at the 2AjB sites.

3.2. B armchair GNR

For the armchair GNR with weak scattering defects, $U = 1.0$ eV, located at the sites of 1AjA, 1AjB, 2AjA, and 2AjB (see Fig. 6), we find that there is almost no influence on the conductances around the Fermi energy, but the conductances are modified in the edge of the channel below the Fermi energy, which can be seen in Figs. 6(a)–6(d). This is because no edge states exist in the armchair GNR, and the scattering strength of the impurities is too small to impact on the conductance.[9]

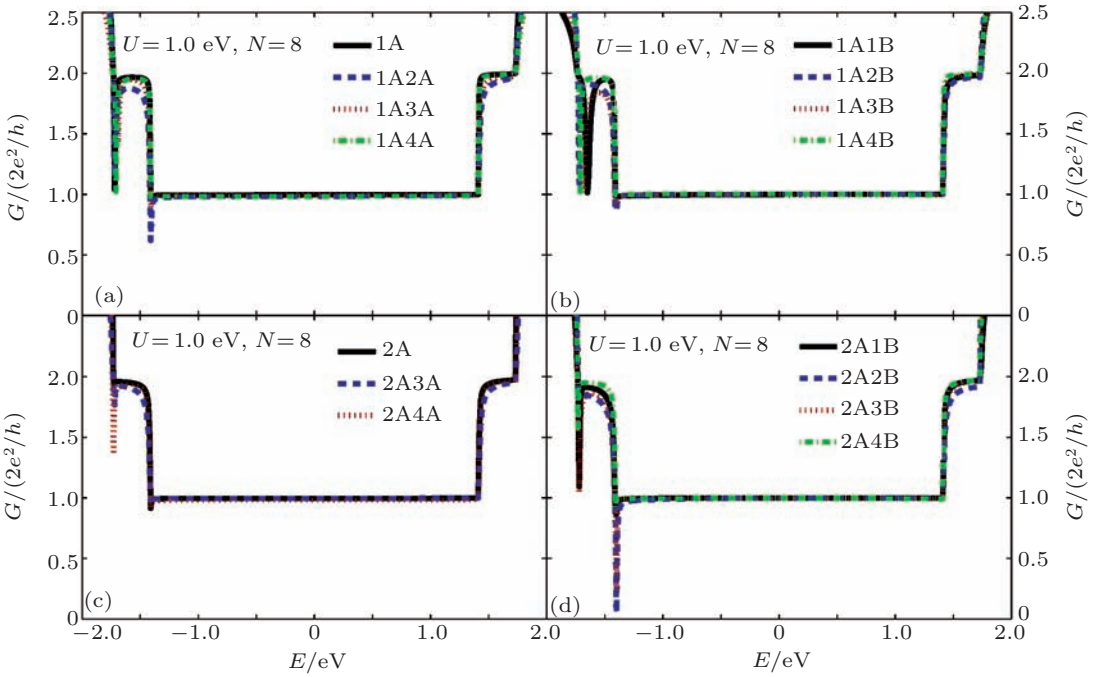


Fig. 6. (colour online) The conductance of the armchair GNR ($N = 8$) at the Fermi energy. (a) One impurity located at the 1A site and two impurities at the 1AjA sites; (b) two impurities located at the 1AjB sites; (c) one impurity located at the 2A, and two impurities at the 2AjA sites; and (d) two impurities located at the 2AjB sites.

For one vacancy at the jA or jB site where $j = 1 \sim 4$, respectively, in Figs. 7(a) and 7(b), the conductance is symmetric and has a dip at the Fermi energy except for the case of the 3A(B)-site vacancy. The pure curves mean the lattice without impurities and defects for comparison.

In Figs. 7(c) and 7(d), the behaviors of the conductances are quite different for the two vacancies at 1AjA or 1AjB. The conductances for the two vacancies at 1AjA still have a dip at the Fermi energy, but two dips appear at the $\pm$1.3 eV channels for the 1AjB-type vacancies. This difference originates from the repulsion effect of the opposite non-bonding characters of two vacancies located at different sublattices, respectively.

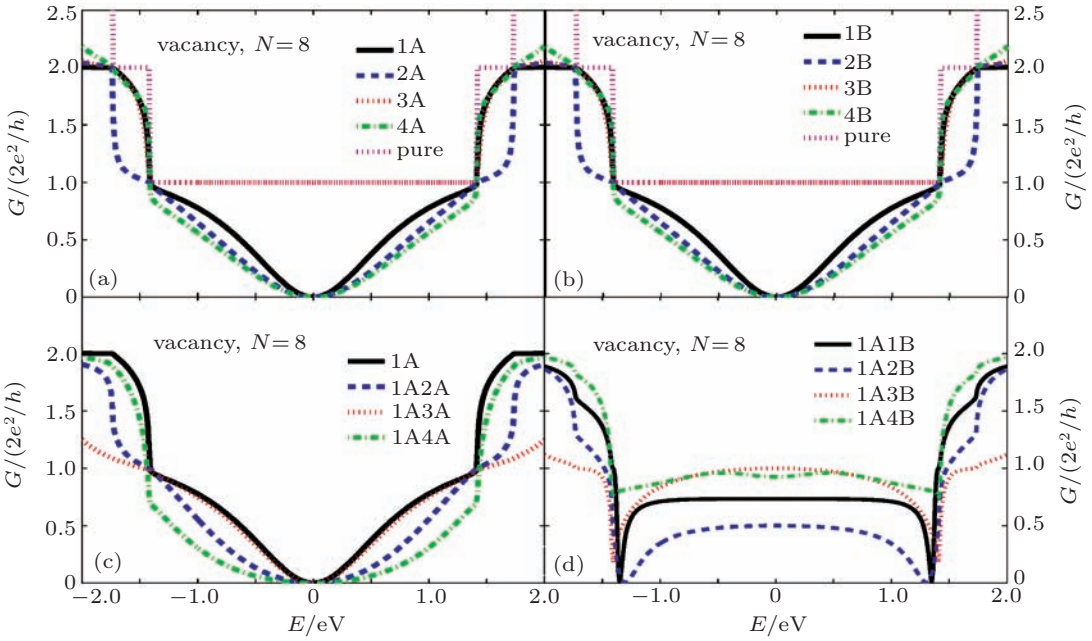


Fig. 7. (colour online) The conductance of the armchair GNR ($N = 8$) near the Fermi energy. One vacancy is located (a) at the jA sites, (b) at the jB sites; (c) two vacancies located at the 1AjA sites (1A for comparison), and (d) at the 1AjB sites.

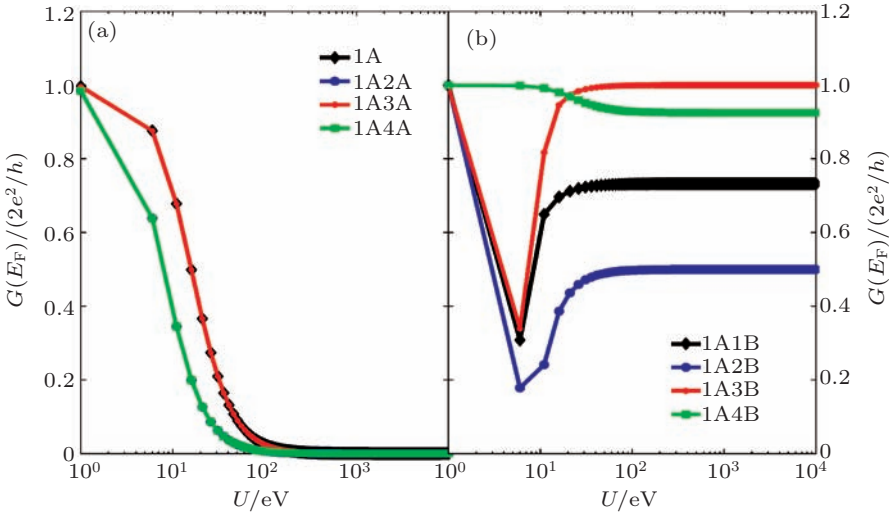


Fig. 8. (colour online) The conductance of the armchair GNR ($N = 8$) at the Fermi energy versus the impurity scattering strength. (a) One impurity located at the 1A site and two at the 1AjA sites; and (b) two impurities located at the 1AjB sites.

Similarly to the zigzag GNR, we plot the conductances at the Fermi energy versus the scattering strength in Figs. 8(a) and 8(b). For one or two vacancies at the A-sublattice, the conductances at the Fermi energy trend to zero for $U > 100$ eV. For two vacancies at the 1AjB sites, the conductances have a dip at $U \approx 8$ eV for $j = 2$ and 3, and trend to constant after $U > 20$ eV, which is similar to the situation of the zigzag GNR. Finally, in Figs. 9(a) and 9(b) we show that the conductances at the Fermi energy versus $1/N$ are related to the width of the GNR. The conductances for one or two vacancies at the A-sublattice increase very slowly with the increase in the width of the GNR, but this is actually very small, 10^{-3} for $N \sim 50$. For two vacancies at the 1AjB sites, the conductances converge to 1 for $j = 1, 2$, and 3, but trend to 0.2 and 0.8 for $j = 4$ and 7, respectively. Actually, the conductances of the GNR with the two vacancies at the 1AjB sites have a periodic behavior with the location of the j sites.[1)] This implies that the conductance in the Fermi energy is sensitive to the location of the two vacancies.

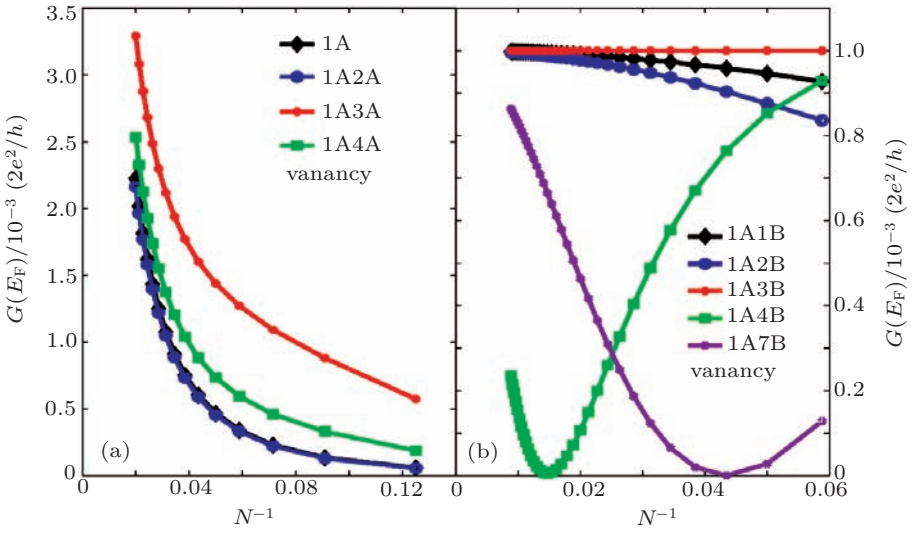


Fig. 9. (colour online) The conductance of the armchair GNR ($N = 8$) at the Fermi energy versus the inverse of the number N of atoms in the width of the GNR. One vacancy is located (a) at the 1A site, and two vacancies at the 1AjA sites; (b) two vacancies located at the 1AjB sites.

It should be pointed out that the above results do not change qualitatively for the defects at iAjA and iAjB, where $i > 2$, even though our calculations are based on the vacancies at $i = 1$ or 2.

4. Conclusion

By numerically studying the transport properties of two typical metallic GNRs with one and two defects based on the tight-binding model with the surface Green's function technique, we reveal the basic physical properties of the conductance near the Fermi energy and their relationships with defect property and location.

For the zigzag GNR with one or two weak scattering impurities, the conductance near the Fermi energy is suppressed due to the quantum confinement effect for the narrow GNR. For one or two vacancies in the narrow zigzag GNR, the conductance near the Fermi energy is also suppressed and shows one or two dips symmetrically near the Fermi energy due to the edge states. The detailed behavior depends on the location of the vacancies. As the width of the GNR increases, the defect effects on the conductance at the Fermi energy become weak and vanish eventually.

For the armchair GNR with one or two weak scattering impurities $U < 1$ eV, the conductance is also independent of impurities at the Fermi energy, but the impurities modify the conductance below the Fermi energy. With the increase in the impurity scattering strength, the conductance in the Fermi energy is suppressed by the AA-type defects, and becomes zero for $U > 100$ eV, which very weakly depends on the width of the GNR. For AB-type defects, the conduc-

[1)] The conductances have periodic behavior for two vacancies at 1AjB, in which the conductances for $j = 1, 2, 3, 5, 6$, and $8, 9, \ldots$ have a similar behavior, and for $j = 4, 7, 10, \ldots$ have another similar behavior.

tance in the Fermi energy shows a dip near $U = 10$ eV and trends to constant with the increase in the impurity scattering strength for the narrow GNR, but the impurity effects become weak and vanish with the increase in GNR width. For one or two vacancies in the armchair GNR, the conductance shows a symmetric behavior in the upper and lower Fermi energy. The couplings between the two defect states have an influence on the conductance. The A-, B-, and AA-type vacancies induce one dip of conductance at the Fermi energy, while the AB-type vacancy leads to two dips of conductance near the Fermi energy due to the opposite non-bonding character of the vacancies. With the increase in the GNR width, the conductance at the Fermi energy has a small increase for the-AA type vacancy, while it shows a periodic behavior for the AB-type vacancy. The effect of the AB-type vacancy tends to vanish for the AB vacancy at 1AjB, except for the periodic position $j = 4, 7, \ldots$, etc. Our results can provide a basic understanding of the defect effect in the transport properties of GNRs, which will be helpful for designing GNR-based nanodevices.

References

[1] Castro Neto A H, Guinea F, Peres N M R, Novoselov K S and Geim A K 2009 *Rev. Mod. Phys.* **81** 1

[2] Ando T 2007 *Int. J. Mod. Phys.* B **21** 1113

[3] Hu H X, Zhang Z H, Liu X H, Qiu M and Ding K H 2009 *Acta Phys. Sin.* **58** 7156 (in Chinese)

[4] OuYang F P, Xu H and Wei C 2008 *Acta Phys. Sin.* **57** 1073 (in Chinese)

[5] Ozyilmaz B, Jarillo-Herrero P, Efetov D and Kim P 2007 *Appl. Phys. Lett.* **91** 192107

[6] Geim A K and Novoselov K S 2007 *Nat. Mater.* **6** 183

[7] Fujita M, Wakabyashi K, Nakada K and Kusakabe K 1996 *J. Phys. Soc. Jpn.* **65** 1920

[8] Nakada K, Fujita M, Dresselhaus G and Dresselhaus M S 1996 *Phys. Rev.* B **54** 17954

[9] Li T C and Lu S P 2008 *Phys. Rev.* B **77** 085408

[10] Wakabayashi K 2004 *J. Phys. Soc. Jpn.* **72** 998

[11] Bahamon D A, Pereira A L C and Schulz P A 2010 *Phys. Rev.* B **82** 165438

[12] Xiong Y J and Kong X L 2010 *Physica* B **405** 1690

[13] OuYang F P, Wang H Y, Li M J, Xiao J and Xu H 2008 *Acta Phys. Sin.* **57** 7132 (in Chinese)

[14] OuYang F P, Wang X J, Zhang H, Xiao J, Chen L N and Xu H 2009 *Acta Phys. Sin.* **58** 5640 (in Chinese)

[15] Chico L, Benedict L X, Louie S G and Cohen M L 1996 *Phys. Rev.* B **54** 2600

[16] Datta S 1996 *Electronic Transport in Mesoscopic Systems* (Cambridge: Cambridge University Press)

[17] Wang L G, Zhang H Y, Wang C and Terence K S W 2010 *Acta Phys. Sin.* **59** 536 (in Chinese)

[18] Krompiewski S, Martinek J and Barnas J 2002 *Phys. Rev.* B **66** 073412

[19] Song H F, Zhu J L and Xiong J J 2002 *Phys. Rev.* B **65** 085408

[20] Kumazaki H and Hirashima D S 2008 *Low Temp. Phys.* **34** 10